Molecular Architecture Effect on the Self-Assembly Behavior of Comb-Coil Block Copolymers Displaying Lamellae-within-Lamellae Morphology

Wei-Shan Chiang,[†] Chia-Hung Lin,[‡] Bhanu Nandan,[†] Chao-Ling Yeh,[†] M. Habibur Rahman,[†,§] Wen-Chang Chen,[‡,∥] and Hsin-Lung Chen*[,†]

Department of Chemical Engineering, National Tsing Hua University, Hsin-Chu 30013, Taiwan, and Department of Chemical Engineering and Institute of Polymer Science and Engineering, National Taiwan University, Taipei 10617, Taiwan

Received May 20, 2008; Revised Manuscript Received July 31, 2008

ABSTRACT: Supramolecular comb-coil block copolymers formed by the stoichiometric complexation of two amphiphilic surfactants, dodecylbenzenesulfonic acid (DBSA) and 3-pentadecylphenol (PDP), with the poly(4-vinylpyridine) (P4VP) blocks in a linear PS-*b*-P4VP and a nonlinear A_nB_n-type heteroarm star PS-P4VP copolymer have been investigated. All linear and heteroarm star systems under study exhibited lamellae-within-lamellae morphology even at high PS volume fraction, at which the previously studied systems showed lamellae-within-cylinder or lamellae-within-sphere morphology. The interlamellar distances of the larger-scale copolymer microdomains were found to be much larger in all heteroarm complexes than those in their linear counterparts. This was attributed to the chain crowding effect coupled with the different types of arrangement of comb blocks forming the smaller-scale lamellar mesophase. Moreover, the order−disorder transition temperatures of both the larger- and smaller-scale structures in the heteroarm star systems were higher than those associated with the linear diblocks due to the lower entropy of transition.

Introduction

Block copolymers constitute a special class of materials capable of self-assembling into a series of long-range ordered nanostructures driven by the incompatibility between the covalently connected blocks.[1] Polymers with comb-shaped architecture also display the propensity to self-organize due to the repulsion between the backbone and the short side chains.[2] The covalent bonds through which the side chains attach to the backbone may be replaced by physical bonds such as ionic bonds,[3,4] hydrogen bonds,[5−7] or metal-mediated coordination bonds[8−10] to yield the "supramolecular comb polymers", which may analogically self-organize to form mesomorphic nanostructures.[11,12]

An even richer variety of ordered nanostructures can be formed if the comb architecture is introduced into the block copolymer by selectively complexing one of the blocks in a coil-coil diblock copolymer with a surfactant.[13] The resultant "supramolecular comb-coil diblock copolymer" displays two distinct levels of self-organization: one gives rise to the larger-length-scale copolymer domain (typically several tens of nanometers) driven by the microphase separation between the comb and coil blocks, and the other yields a smaller-length-scale lamellar structure (with interlamellar distances of several nanometers) due to the segregation between the polymer backbone and surfactant tails in the comb block. "Structure-within-structure" is an appropriate term for describing such a morphological pattern. Moreover, due to the presence of two structure units with different length scales, two order−disorder transition (ODT) temperatures (T_{ODT}) can be defined for the comb-coil copolymers, namely, T_{ODT}^{L} and T_{ODT}^{S}, corresponding to T_{ODT} of the larger-scale copolymer domain and the smaller-scale mesophase organized by the comb block, respectively.[14,15]

The supramolecular comb-coil concept was pioneered and widely investigated by Ikkala and co-workers.[5,8,10,13,16−23] In addition to the rich variety of hierarchical nanostructures, the mesomorphic order of the comb block also exerts interesting influence on the self-organization behavior of the coil block. For instance, the smaller-scale lamellar mesophase was found to induce anomalous tetragonal packing of the larger-scale cylindrical domains organized by the coil block in a supramolecular comb-coil diblock formed by complexation of polystyrene-*block*-poly(4-vinylpyridine) (PS-*b*-P4VP) with dodecylbenzenesulfonic acid (DBSA).[24]

With the advancement of synthetic techniques, block copolymers with nonlinear architectures, including heteroarm star,[14,25−30] block-arm star, H-shaped, and π-shaped,[31,32] are now brought into investigation. Recently, we have been interested in the microphase separation and ODT of supramolecular comb-coil copolymers bearing nonlinear architecture.[14,15] It is known that the nonlinear copolymers also self-assemble to form well-ordered nanostructures; however, remarkable differences in ODT and domain spacing from those of the linear counterpart have been observed.[1,25−30] We therefore expect that introducing nonlinear architecture into the supramolecular comb-coil systems may also influence their phase behavior considerably.

In a previous study,[15] we investigated a nonlinear comb-coil copolymer formed by an A_nB_n-type heteroarm polystyrene−poly(2-vinylpyridine) (PS-P2VP) with the P2VP block complexed with DBSA. The system displayed PS cylinder-within-lamellae morphology due to low PS volume fraction. A reduction of interdomain distance and a significant increase of T_{ODT}^{S} were observed in the heteroarm system as compared with its linear counterpart. In this study, we proceeded further to study the microphase separation behavior of the copolymer systems with intermediate and high volume fractions of the PS coil block. Here the comb-coil copolymers were formed by complexing the P4VP block in linear PS-*b*-P4VP and heteroarm PS-P4VP

* To whom correspondence should be addressed: e-mail hslchen@mx.nthu.edu.tw.
[†] National Tsing Hua University.
[‡] Department of Chemical Engineering, National Taiwan University.
[§] On leave from the Department of Chemistry, University of Rajshahi, Rajshahi 6205, Bangladesh.
[∥] Institute of Polymer Science and Engineering, National Taiwan University.

10.1021/ma801116h CCC: $40.75
Published on Web 10/08/2008

Table 1. Characteristics of PS-P4VP Copolymers and Their Complexes with DBSA and PDP

	M_n					f_{PS}		
sample[a]	overall[b]	PS block or arm[c]	P4VP block or arm[d]	M_w/M_n	n[e]	before	DBSA complex[f]	PDP complex[g]
L1	20 880	15 230	5650	1.06		0.73	0.40	0.41
H1	67 240	15 790	4900	1.17	6.5	0.76	0.44	0.45
L2	18 390	17 100	1290	1.05		0.93	0.76	
H2	59 640	16 960	1390	1.11	6.5	0.92	0.75	

[a] **LX** and **HX** (X = 1 or 2) represent linear diblock and heteroarm star copolymers, respectively. [b] Number-average molecular weight of whole copolymer measured by GPC. [c] Number-average molecular weight per PS block or arm. [d] Number-average molecular weight per P4VP block or arm. [e] Average number of PS or P4VP arms of the heteroarm star copolymer. [f] Overall volume fraction of PS in the copolymers after complexation with DBSA. [g] Overall volume fraction of PS in the copolymers after complexation with PDP.

with DBSA or 3-pentadecylphenol (PDP). Previous studies have demonstrated that DBSA and PDP formed complexes with P4VP through ionic and hydrogen bonding, respectively.[22−24] It will be shown here that all the copolymer complexes under study exhibited the lamellae-within-lamellae morphology even at high PS volume fraction, at which the previously studied systems showed lamellae-within-cylinder or lamellae-within-sphere morphology. Moreover, in contrast to our previously studied comb-coil copolymers showing cylinder-within-lamellae morphology,[15] the present heteroarm complexes displayed a much larger interdomain distance than their linear counterparts. The results indicated that the influence of molecular architecture is quite complex, as it depends on the type of hierarchical structure formed.

Experimental Section

1. Synthesis of PS-P4VP Copolymers. Detailed synthetic procedures for the block copolymers employed in this study have been given in the Supporting Information. In short, linear PS-*b*-P4VP was synthesized by sequential living anionic polymerization.[33] Two linear PS-*b*-P4VP copolymers were prepared and denoted as **L1** and **L2.** The molecular characteristics of these materials are tabulated in Table 1. A three-step sequential copolymerization was used to prepare heteroarm star PS_n-$P4VP_n$, where n represents the arm numbers of the star copolymer. The synthetic scheme was similar to that of heteroarm star PS-P2VP reported in our previous study.[15] Two heteroarm star copolymers were prepared and denoted as **H1** and **H2.** The detailed characteristics of the heteroarm copolymers are also listed in Table 1.

2. Complex Preparation. Dodecylbenzenesulfonic acid (DBSA, Acros, mixture of C10∼C13 isomers) was used without further purification, and 3-pentadecylphenol (PDP, Aldrich, tech. 90%) was purified by recrystallization from petroleum ether. For preparation of complexes of the copolymers with DBSA and PDP, the copolymers and surfactants were first dissolved separately in chloroform to the concentration of 3 wt % to form clear solutions. The complexes were then prepared by mixing appropriate quantities of the two solutions, which would prescribe the stoichiometric binding of the surfactants to P4VP block. Most of the solvent was evaporated at room temperature. Finally, the samples were dried under vacuum at 60 °C for 48 h to remove the residual solvent. All the complexes with DBSA were further annealed at 140 °C for 48 h to enhance the long-range order of the copolymer domains.

3. Small-Angle X-Ray Scattering Measurements. Temperature-dependent small-angle X-ray scattering (SAXS) experiments in a heating cycle were conducted to probe the morphologies of the copolymers. The samples were first equilibrated for 20 min, followed by data acquisition for 1 h at each measuring temperature under vacuum. The SAXS instrument was equipped with a 3.0 kW X-ray generator operated at 40 kV × 35 mA (Nanostar, Bruker Co. Ltd.) and a two-dimensional position-sensitive proportional counter with 512 × 512 channels. The Cu Kα line ($\lambda = 0.154$ nm) was used. The intensity profile was output as the plot of the scattering intensity (I) versus the scattering vector, $q = (4\pi/\lambda) \sin(\theta/2)$, where θ is the scattering angle. All data were corrected by empty beam scattering, the sensitivity of each pixel of the area detector, and thermal diffuse scattering (TDS).

4. Transmission Electron Microscope Observations. Real-space morphologies were observed by use of a JEOL JEM-2000FXZ transmission electron microscope (TEM) operated at 100 kV. The copolymer specimens were microtomed at −60 °C with a Reichert Ultracut E low-temperature sectioning system. The microtomed sections were collected onto copper grids coated with carbon-supporting films and then stained for 10 min in RuO_4 vapor. Since RuO_4 was a preferential staining agent for PS, the PS- and P4VP-containing domains appeared as dark and bright regions in the micrographs, respectively.

5. Differential Scanning Calorimetry Measurements. The phase transitions of PDP in the complexes were investigated by a TA Instrument 2000 differential scanning calorimeter (DSC). The samples were heated from 30 to 100 °C with a heating rate of 20 °C/min.

Results

1. Comb-Coil Copolymers with Hydrogen-Bonding Complexation: A. L1(PDP) System. Figure 1a,b displays temperature-dependent SAXS profiles of the **L1(PDP)** system in the temperature range of 30−200 °C. The SAXS profile at 30 °C showed a scattering maximum at $q = 0.31$ nm^{-1}. A broad peak superposing with a few relatively sharp peaks was observed in the high-q region ($q \approx 1.6$ nm^{-1}). The low-q peak, corresponding to domain spacing of 20.27 nm, was associated with the larger-scale copolymer domain structure arising from microphase separation between PS and P4VP(PDP) blocks. The high-q peaks were contributed by the smaller-scale structure organized by the P4VP(PDP) comb blocks. It was difficult to identify the copolymer microdomain morphology due to the lack of higher-order peaks. Consequently, the copolymer domain structure was revealed by TEM. The TEM micrograph in Figure 2 shows the formation of lamellar microdomains in **L1(PDP)**.

Upon heating over 70 °C, the intensity of the low-q peak decreased progressively, as demonstrated from the I_m^{-1}(L) versus T^{-1} plot in Figure 1c, where I_m(L) signifies the low-q peak intensity. Two onsets of obvious intensity changes were identified at ca. 70 and 120 °C. The steep decrease of I_m(L) above 120 °C was attributed to the disordering of the copolymer domains; that is, $T_{ODT}^{L} \approx 120$ °C.

For the high-q peaks associated with the smaller-scale structure, sharp peaks superposing on the broad one were observed at 30 °C. The sharp peaks vanished on heating above 50 °C. The high-q feature in the SAXS profile observed for the present system was quite different from that observed for the complex of P4VP homopolymer (h-P4VP) with PDP. The reported SAXS profiles of h-P4VP(PDP) showed only a single sharp scattering peak below T_{ODT} until the crystallization of PDP started near 20 °C.[34] Once PDP crystallization started, the scattering curve contained the contribution from both h-P4VP(PDP) mesophase and PDP crystals. Hence, the scattering peaks observed in the high-q region at 30−50 °C for **L1(PDP)** complexes needed further investigation. It must be noted that macrophase separation of PDP was ruled out in this case since the crystallization of pure PDP would lead to a long period of

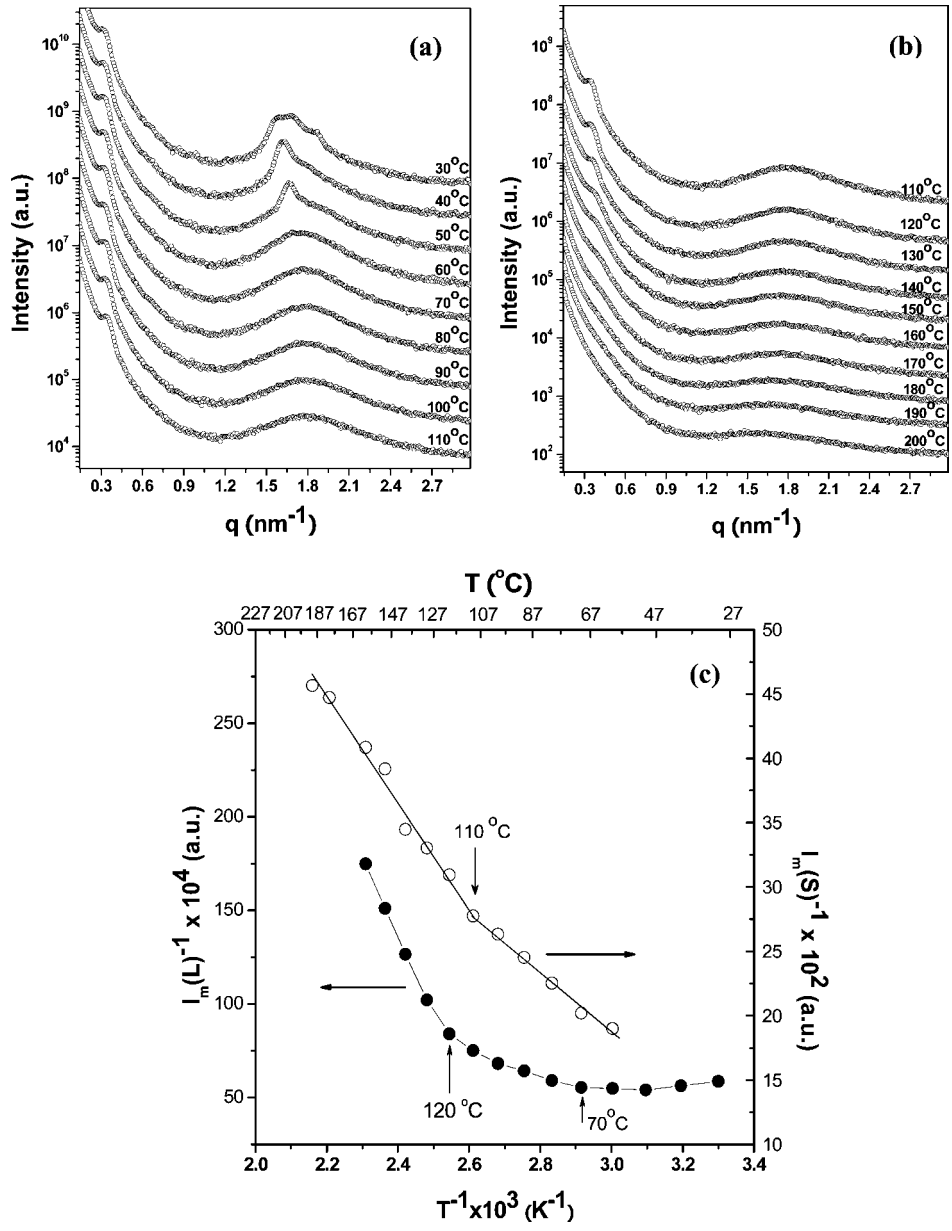

Figure 1. Temperature-dependent SAXS profiles of **L1(PDP)** collected in situ from (a) 30 to 110 °C and (b) 110 to 200 °C in a heating cycle; (c) I_m^{-1}(L) (●) and I_m^{-1}(S) (○) vs T^{-1} plots for assessing the order−disorder transition temperatures (T_{ODT}) of **L1(PDP)**. I_m(L) and I_m(S) correspond to the intensities of the primary scattering peaks associated with the larger- and smaller-scale structures, respectively.

~2.7 nm, which should be identified in the scattering data with a peak at 2.3 nm^{-1}. However, no such peak was observed in the scattering profile of **L1(PDP)**.

A DSC heating scan was conducted to assist in elucidation of the phase behavior of PDP in the **L1(PDP)** complex. Figure 3 shows the DSC thermogram of **L1(PDP)** obtained at a heating rate of 20 °C/min. A large endotherm (with enthalpy of transition $\Delta H_t \sim 18$ J/g) due to the melting of the crystals formed by the P4VP-bound PDP was identified at 21.8 °C. This was similar to that reported for the hydrogen-bonded PDP.[35,36] However, careful observation of the DSC data showed that the melting process of PDP was not completed until about 50 °C. This indicated that PDP crystallites were always present up to ca. 50 °C. Hence, when the temperature was lower than 50 °C, P4VP(PDP) blocks formed a lamellar morphology (with interlameller distance $d \sim 3.6$ nm) consisting of alternating P4VP backbone and PDP layer. The PDP layers exhibited some degree of crystallinity, and the presence of the PDP crystallites gave rise to the sharp peak superposing on the broad one in the high-q region of the SAXS profiles. Above 50 °C, this lamellar structure transformed into a mesophase in which the PDP molecules were no longer crystalline.

Figure 3 revealed another small endotherm situated at 71.2 °C for **L1(PDP)**. This endothermic event was attributable to the transition from the mesophase to an isotropic phase, namely, the ODT of the smaller-scale mesophase organized by the comb block ($T^S_{ODT} \approx 71.2$ °C). This temperature coincided well with the first onset temperature at which the low-q peak intensity dropped obviously (cf. Figure 1c). The remaining broad SAXS peak in the high-q region above 70 °C was considered as the "correlation hole" peak reflecting the concentration fluctuations in the disordered comb block microdomains.

Figure 1c also displays the change of the high-q peak intensity [I_m(S)] at temperatures above 70 °C. I_m(S) was found to decrease monotonically with increasing temperature, but a steeper drop was identified above 110 °C, which lies closer to T^L_{ODT}. We considered this temperature as the one at which the detached PDP molecules (due to breakage of hydrogen bonds) in the disordered comb block domains started to diffuse into

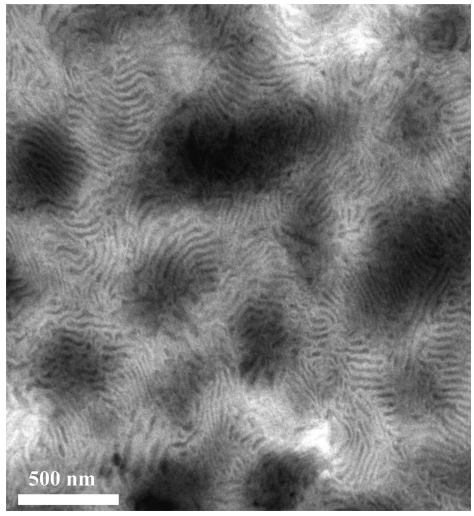

Figure 2. TEM micrograph showing the formation of lamellar copolymer domains in **L1(PDP)**.

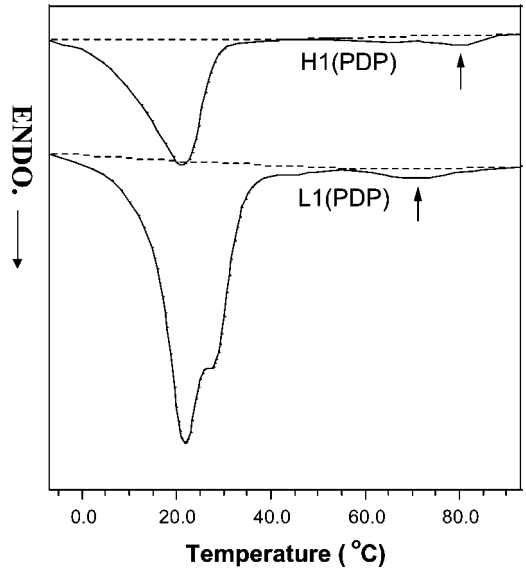

Figure 3. DSC heating curves of **L1(PDP)** and **H1(PDP)** with a heating rate of 20 °C/min. The small endotherms associated with the mesophase−isotropic phase transition are marked by arrows.

the PS domains, which eventually homogenized the whole system.

Figure 4 shows temperature-dependent SAXS profiles of the **L1(PDP)** system obtained during subsequent cooling experiment from 200 to 30 °C. The reappearance of scattering peaks at both low- and high-q regions during cooling showed that the structural features described above were thermally reversible. The thermal reversibility observed also showed that the sample was thermally stable under the experimental conditions employed for the SAXS experiments.

B. H1(PDP) System. Figure 5a,b shows the temperature-dependent SAXS profiles of the **H1(PDP)** system. The scattering curves at low temperatures showed a primary maximum at 0.21 nm^{-1} and two weak higher-order peaks at 0.42 and 0.66 nm^{-1}. Another peak with strong intensity was observed in the high-q region at 1.62 nm^{-1}. Similarly, the SAXS peaks in the low-q region were attributed to the larger-scale copolymer domain structure. The integral ratio of the peak positions signaled the formation of a lamellar morphology with interlamellar distance $D = 29.92$ nm consisting of alternating PS and P4VP(PDP)

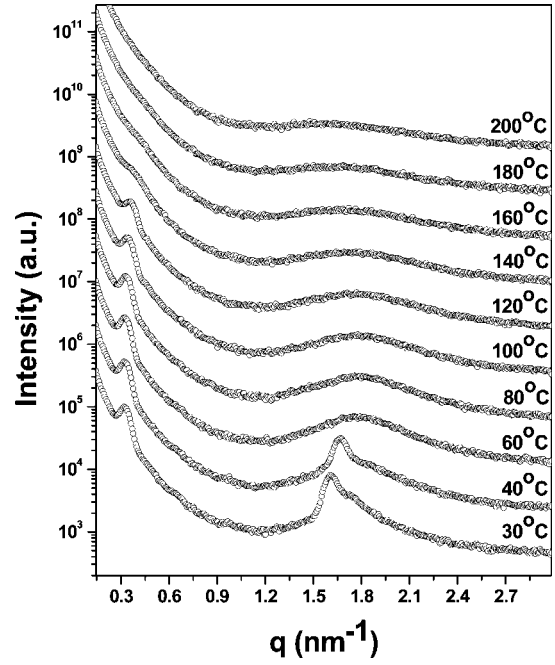

Figure 4. Temperature-dependent SAXS profiles of **L1(PDP)** collected in situ from 200 to 30 °C in a cooling cycle.

layers. This morphology was expected from the rather symmetric composition of the comb-coil copolymer ($f_{PS} = 0.45$).

The high-q peak at 1.62 nm^{-1} stemmed from the smaller-scale lamellar mesophase formed by P4VP(PDP) combs with $d = 3.9$ nm. Hence, the **H1(PDP)** system also self-organized into a lamellae-within-lamellae morphology. Upon heating to 80 °C, the intensity of the high-q peak dropped sharply [cf. $I_m^{-1}(S)$ vs T^{-1} plot in Figure 5c] coupled with peak broadening, signaling that the lamellar mesophase underwent an ODT (i.e., $T_{ODT}^{S} \approx 80$ °C). This ODT event was confirmed by the DSC thermogram in Figure 3, showing a small endotherm at 79.7 °C due to the transition from mesophase to isotropic phase for the P4VP(PDP) comb blocks. The DSC thermogram also showed a larger endotherm ($\Delta H_t \sim 10$ J/g) at 21.2 °C, which was attributed to the melting of PDP crystallites. It should, however, be noted that the PDP crystallites in this system completely melted below 30 °C and hence the SAXS profile collected at the lowest temperature in Figure 5a (40 °C) did not show the sharp peak associated with the PDP crystallites superposing on the broader peak in the high-q region.

As can be seen in Figure 5c, $I_m(L)$ did not show any abrupt decrease up to 170 °C and hence the larger-scale copolymer domains were stable up to at least 170 °C (i.e., $T_{ODT}^{L} > 170$ °C). The SAXS profiles collected in a subsequent cooling experiment also demonstrated that the structural features were thermally reversible (cf. Supporting Information). Hence, both T_{ODT}^{L} and T_{ODT}^{S} of **H1(PDP)** were higher than those of **L1(PDP)**, which was consistent with our previous results on the PS-P2VP(DBSA) systems displaying cylinder-within-lamellae morphology, showing that the introduction of nonlinear architecture increased T_{ODT} of the structures at both length scales.[15]

2. Comb-Coil Copolymers with Ionic Complexation: A. L1(DBSA) System. Figure 6 shows the temperature-dependent SAXS profiles of the **L1(DBSA)** system. The scattering patterns in the low-q region were characterized by a primary maximum at 0.31 nm^{-1} and a second-order peak at 0.63 nm^{-1}, showing the formation of a larger-scale lamellar structure with $D = 20.27$ nm due to the microphase separation between PS and P4VP(DBSA) blocks. Another peak of strong intensity observed at 2.01 nm^{-1} was associated with the lamellar mesophase with

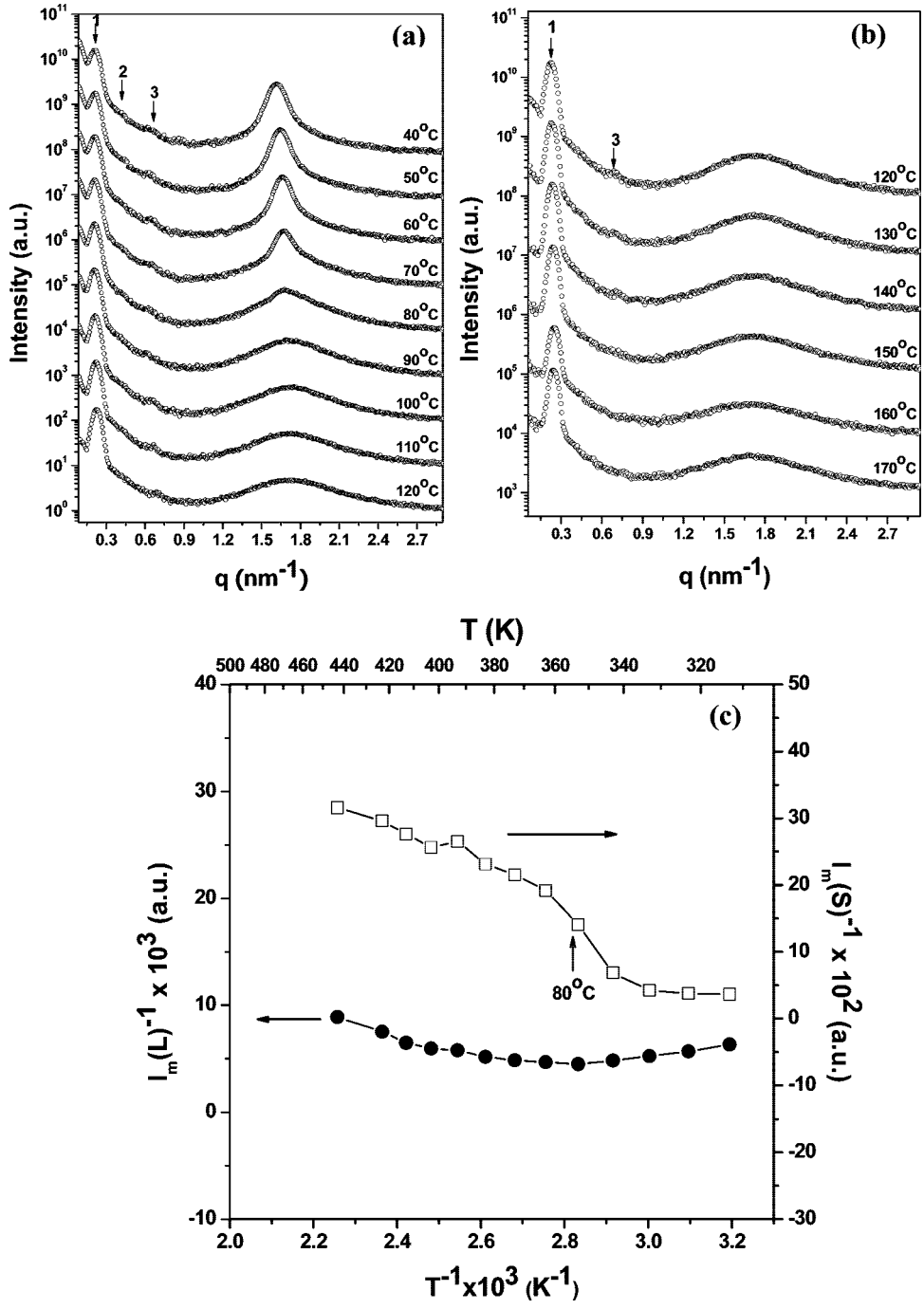

Figure 5. Temperature-dependent SAXS profiles of **H1(PDP)** collected in situ from (a) 40 to 120 °C and (b) 120 to 200 °C in a heating cycle; (c) I_m^{-1}(L) (●) and I_m^{-1}(S) (□) vs T^{-1} plots for assessing the order−disorder transition temperatures (T_{ODT}) of **H1(PDP)**. I_m(L) and I_m(S) correspond to the intensities of primary scattering peaks associated with the larger- and smaller-scale structures, respectively.

d = 3.13 nm formed by the P4VP(DBSA) comb blocks. Consequently, the **L1(DBSA)** complex also displayed a lamellae-within-lamellae morphology.

The temperature-dependent experiment indicated no ODT in either larger- or smaller-scale structures upon heating from 30 to 240 °C. Therefore, both T_{ODT}^{S} and T_{ODT}^{L} of **L1(DBSA)** were significantly higher than those of **L1(PDP)** due to the stronger polar−nonpolar repulsion associated with ionic complexation.

B. H1(DBSA) System. Figure 7 shows the temperature-dependent SAXS profiles of the **H1(DBSA)** complex in the temperature range of 30−240 °C. The SAXS profile at 30 °C showed a first-order scattering peak at 0.18 nm^{-1} and a second-order peak which again demonstrated the formation of a larger-scale lamellar morphology with D = 34.91 nm. Another strong peak in the high-q region associated with the P4VP(DBSA) lamellar mesophase was located at 2.29 nm^{-1}. Consequently, the **H1(DBSA)** complex also self-assembled into a lamellae-within-lamellae morphology. The SAXS heating experiment also indicated that **H1(DBSA)** exhibited higher T_{ODT}^{S} and T_{ODT}^{L} than **H1(PDP)**, as no ODT was detectable up to 240 °C.

C. L2(DBSA) System. Figure 8a presents temperature-dependent SAXS profiles of the **L2(DBSA)** complex. Below 200 °C the scattering curves displayed up to six diffraction peaks with integral position ratio, signaling that PS blocks and P4VP(DBSA) combs microphase separated to form a highly ordered lamellar structure with D = 20.07 nm. It was intriguing that a lamellar morphology was formed even though the

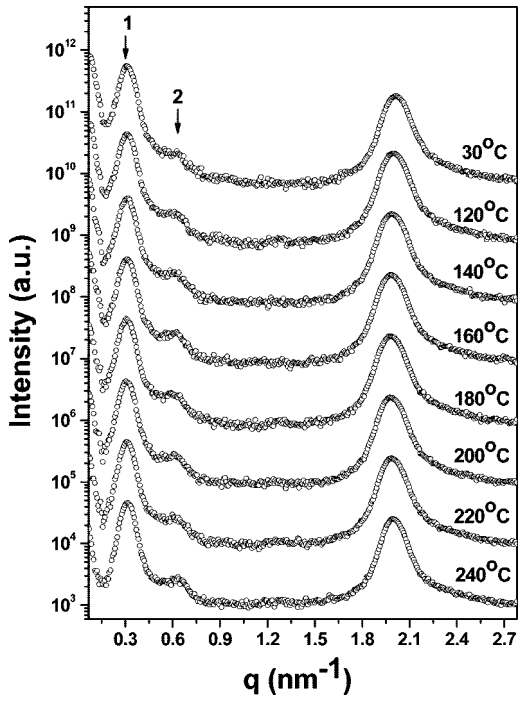

Figure 6. Temperature-dependent SAXS profiles of **L1(DBSA)** collected in situ from 30 to 240 °C in a heating cycle.

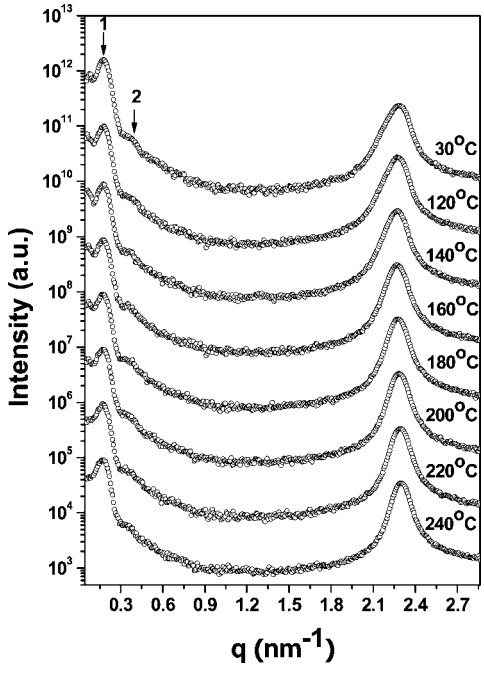

Figure 7. Temperature-dependent SAXS profile of **H1(DBSA)** collected in situ from 30 to 240 °C in a heating cycle.

corresponding f_{PS} was 0.76, which fell in the region of cylindrical morphology in the regular phase diagram of coil-coil diblock copolymer.[37−39] The high-q peak associated with the smaller-scale structure was very broad. This suggested that the smaller-scale lamellar structure organized by P4VP(DBSA) comb block was poorly ordered. It must be mentioned that the broad peak was not a correlation hole peak, because the slope of the tail region of this peak in the double-log plot was ca. −4. This corresponded to the scattering from a two-phase system with sharp phase boundary prescribed by Porod's law.[40,41] Moreover, as will be described below, a sharp drop in intensity of this peak was observed near 220 °C, showing that an ODT

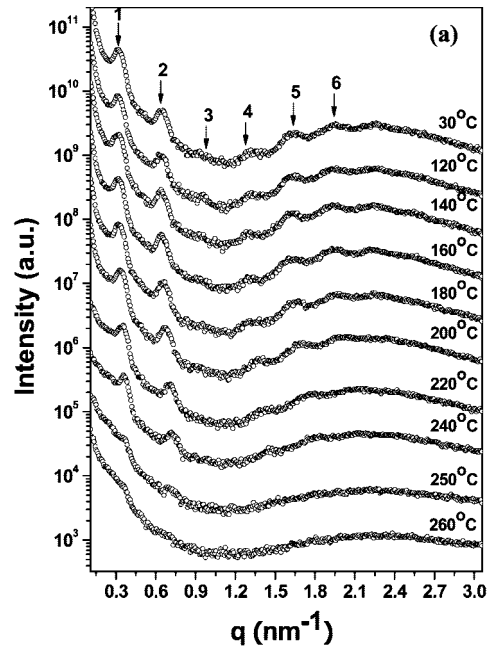

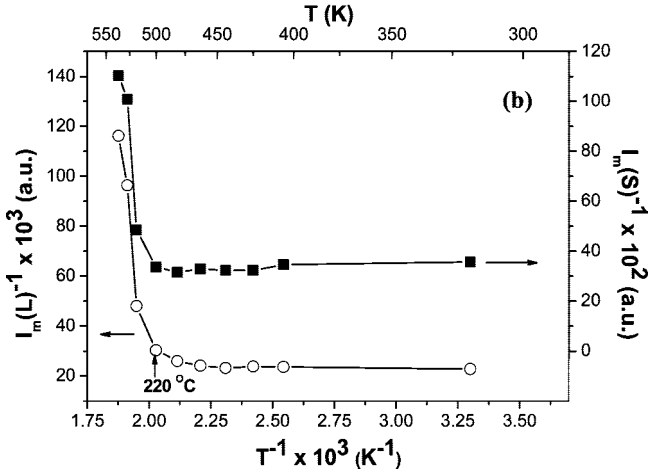

Figure 8. (a) Temperature-dependent SAXS profile of **L2(DBSA)** collected in situ from 30 to 260 °C in a heating cycle; (b) I_m^{-1}(L) (○) and I_m^{-1}(S) (■) vs T^{-1} plots, with I_m(L) and I_m(S) corresponding to the intensities of primary scattering peaks associated with the larger- and smaller-scale structures, respectively.

of the smaller-scale structure existed in this sample near this temperature (also see Supporting Information). Such a discontinuous drop in intensity was not prescribed for a correlation hole peak.

Figure 8b presents the I_m^{-1} versus T^{-1} plots for the primary scattering maxima associated with the larger- and smaller-scale structures. Abrupt drops of intensities were identified near 220 °C in both cases, indicating that the disordering of the larger-scale lamellar structure (ODT^L) occurred almost concurrently with that of the smaller-scale mesophase (ODT^S); that is, $T_{ODT}^L \approx T_{ODT}^S \approx 220$ °C. In this case, the occurrence of ODT^L induced mixing between the coil and comb blocks, and hence disrupted the smaller-scale structure simultaneously.

Figure 9 shows the temperature-dependent SAXS profiles of **L2(DBSA)** obtained during subsequent cooling from 260 to 30 °C. The scattering peaks in both low- and high-q regions reappeared during cooling, which showed that the structural features described above were thermally reversible.

D. H2(DBSA) System. Figure 10a shows the temperature-dependent SAXS profiles of **H2(DBSA)**. The scattering pattern

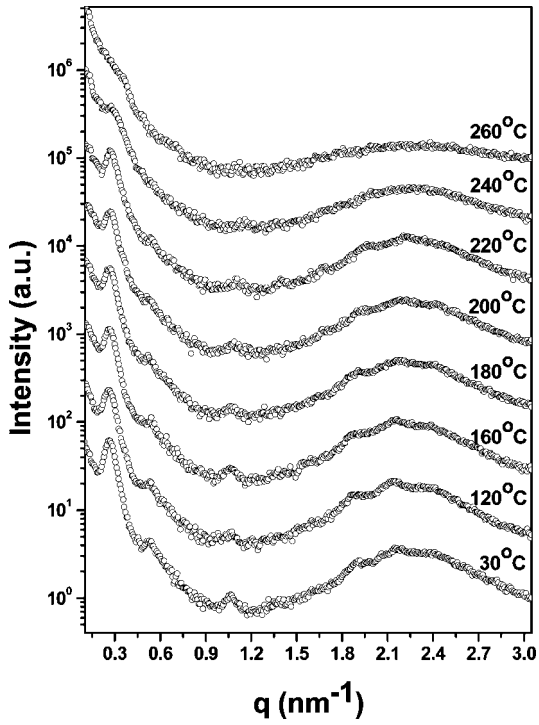

Figure 9. Temperature-dependent SAXS profiles of **L2(DBSA)** collected in situ from 260 to 30 °C in a cooling cycle.

showed a primary maximum associated with the larger-scale structure at 0.22 nm^{-1} and another strong peak of the smaller-scale mesophase at 2.33 nm^{-1}. The inset shows the Lorentz-corrected Iq^2 versus q plot at 30 °C in the low-q region. It can be seen that a weak second-order peak became visible, which signaled that the system formed a larger-scale lamellar morphology with $D \approx 28.56$ nm. This was further corroborrated from the SAXS data obtained from a synchrotron radiation facility (cf. Supporting Information). Consequently, **H2(DBSA)** also exhibited the lamellae-within-lamellae morphology. Again, it was rather unexpected that **H2(DBSA)** with $f_{PS} = 0.75$ could self-organize into a larger-scale lamellar morphology. Another interesting feature worth noting was that though **H2(DBSA)** displayed a less ordered larger-scale lamellar structure than **L2(DBSA)**, its smaller-scale mesophase was more ordered, as demonstrated by a sharper high-q peak.

Figure 10b shows the corresponding $I_m(L)^{-1}$ and $I_m(S)^{-1}$ versus T^{-1} plots. Although $I_m(L)$ and $I_m(S)$ decreased above 200 °C, the intensity changes were indeed small compared with those found in Figure 8b for **L2(DBSA)**. Consequently, we concluded that the morphology of **H2(DBSA)** was much more stable than that of **L2(DBSA)**, as the ODTs were not accessible up to 260 °C. This result was again consistent with our previous study, showing that the order−disorder transition temperatures of the comb-coil copolymer with star architecture were higher than those of the linear counterparts.Table 2 summarizes the morphological parameters and T_{ODT} values of the six systems studied. All copolymers were found to display lamellae-within-lamellae morphology.

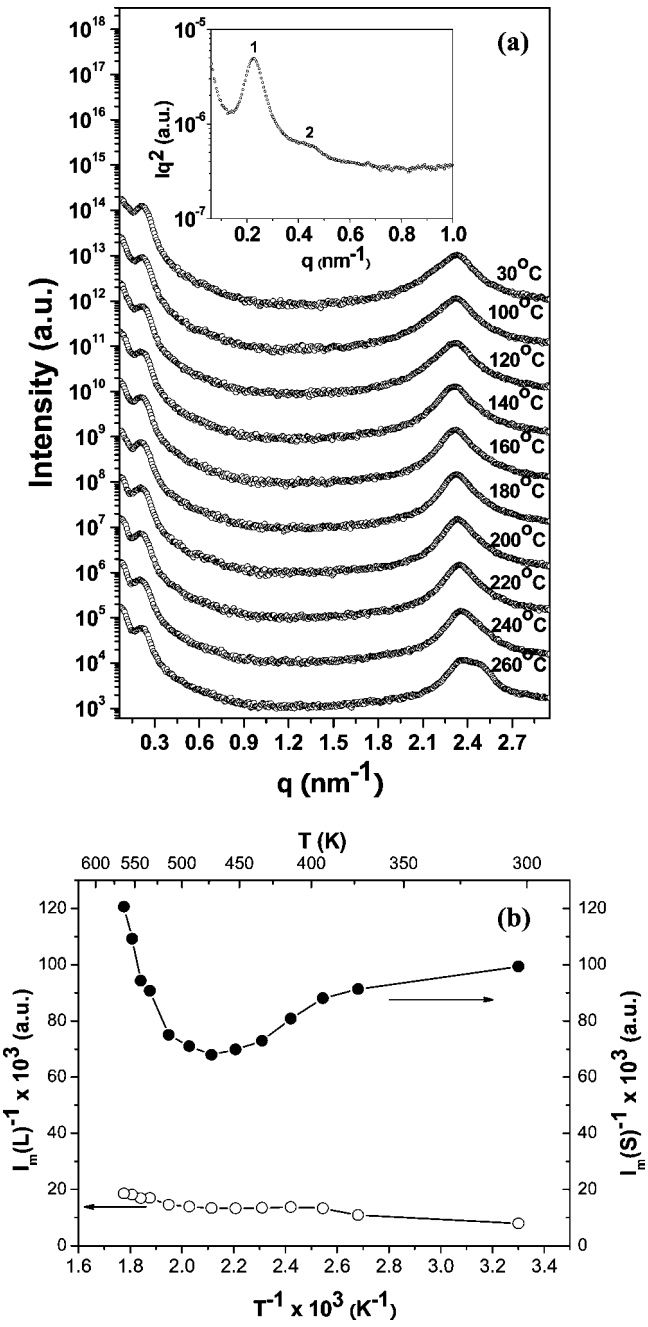

Figure 10. (a) Temperature-dependent SAXS profile of **H2(DBSA)** collected in situ from 30 to 260 °C in a heating cycle. (b) $I_m^{-1}(L)$ (○) and $I_m^{-1}(S)$ (●) vs T^{-1} plots, with $I_m(L)$ and $I_m(S)$ corresponding to the intensities of primary scattering peaks associated with the larger- and smaller-scale structures, respectively.

Discussion

1. L1(PDP) versus H1(PDP). The molecular weights and compositions of **L1** and **H1** were very similar. Therefore, a close comparison between the self-assembly behavior of **L1(PDP)** and **H1(PDP)** would allow the molecular architecture effect on the hydrogen-bonded systems to be revealed. **H1(PDP)** was found to exhibit both higher $T_{ODT}^{\downarrow}$ and T_{ODT}^{δ} than **L1(PDP)**. This phenomenon can be attributed to the lower entropy of transition arising from the localization of junction points in the heteroarm star system.[15]

SAXS (Figure 1) and DSC (Figure 3) results revealed that PDP in **L1(PDP)** exhibited a certain degree of crystallinity even at 30 °C and transformed completely into the mesophase above 50 °C. However, PDP in **H1(PDP)** melted completely before 30 °C. Moreover, the observed enthalpy of melting of PDP crystals in **L1(PDP)** was ∼18 J/g, whereas that for **H1(PDP)** was only ∼10 J/g. The DSC results thus showed that the PDP crystals in **H1(PDP)** were probably less stable and the fraction of PDP involved in crystallization was lower compared to that in **L1(PDP)**. This could be understood from the junction point effect in the heteroarm copolymers. The crowding of a larger number of arms radiating from the junction points may hinder

Table 2. Morphological Characteristics of the Comb-Coil Systems under Study

sample	f_{PS}	D^a (nm)	d^b (nm)	T_{ODT}^L (°C)	T_{ODT}^S (°C)	Σ^c(nm^2)
L1(PDP)	0.41	20.27	3.64	120	71.2	5.71
H1(PDP)	0.45	29.92	3.88	>170	79.7	3.77
L1(DBSA)	0.40	20.27	3.13	>240	>240	5.99
H1(DBSA)	0.44	34.91	2.74	>240	>240	3.21
L2(DBSA)	0.76	20.07	2.87	220	220	3.54
H2(DBSA)	0.75	28.56	2.70	>260	>260	2.43

[a] Interlamellar distance of larger-scale copolymer domains. [b] Interlamellar distance of smaller-scale lamellar mesophase organized by the comb blocks. [c] Average cross section allocated for a PS block (or a comb block) calculated by $\Sigma = 2m_{PS}/(D_{PS}\rho_{PS})$, where m_{PS} is the mass of a PS block chain, D_{PS} is the thickness of the PS lamellar microdomain, and ρ_{PS} is the density of PS. D_{PS} is divided by 2 since we assume that PS blocks adopted a double-layered arrangement.

the PDP molecules attached to P4VP blocks from orderly packing into a crystalline state near the junction points (or near the interface of the copolymer domains). Such an obstacle for crystallographic packing may be gradually alleviated from the interface to the center of the lamellar microdomain. As a result, only the PDP chains far away from the junction point participated in the crystallization process.

The SAXS profiles at a given temperature (e.g., 60 °C) in Figures 1 and 5 further indicated that the orderings of both the larger- and smaller-scale structures were better in **H1(PDP)** than those in **L1(PDP)**. The poorer ordering of the larger-scale structure in **L1(PDP)** was due to perturbation by the higher extent of crystallization of PDP in the system. It is known that the crystallization may perturb the long-range order of the melt mesophase of block coolymers.[42,43] For **L1(PDP)**, the crystallization of PDP during solvent casting (for complex preparation) may perturb the ordering of PS microdomains above the critical concentration for microphase separation. The long-range order did not recover upon heating to 60 °C, by which the PDP crystals in the comb block domains completely melted, since the temperature was still lower than the T_g of PS. But above the T_g of PS blocks, the P4VP(PDP) lamellar mesophase had already been disrupted and a fraction of PDP molecules dissociated from P4VP blocks diffused into PS domains, which eventually homogenized the whole system.

2. L1(DBSA) versus H1(DBSA). In our experimental temperature range of 30−240 °C, **L1(DBSA)** and **H1(DBSA)** exhibited neither ODT^L nor ODT^S, indicating that both T_{ODT}^L and T_{ODT}^S were greatly increased when the binding surfactant changed from PDP to DBSA. The significant increases of T_{ODT} values were due to the stronger polar−nonpolar repulsions associated with the presence of ionic moiety. Normally, ionic bonds may result in T_{ODT} close to or even higher than the thermal decomposition temperature of the block copolymer system.

3. L2(DBSA) versus H2(DBSA). It is surprising that both **L2(DBSA)** and **H2(DBSA)**, with $f_{PS} = 0.76$ and 0.75, respectively, formed lamellae-within-lamellae morphology. Ruokolainen et al.[17] had investigated a series of linear PS-*b*-P4VP(nonadecylphenol) [PS-P4VP(NDP)] comb-coil copolymers with different compositions. The systems with $f_{PS} = 0.75$ and 0.76 were found to display lamellae-within-cylinder or lamellae-within-sphere morphology; namely, the comb block formed cylindrical or spherical microdomains dispersed in the PS matrix. Due to the same kind of block copolymer being used, the unexpected lamellae-within-lamellae morphology of **L2(DBSA)** was attributed to the very short P4VP blocks ($M_n = 1290$) in the PS-*b*-P4VP used here. To form a lamellae-within-cylinder or lamellae-within-sphere morphology, the P4VP(DBSA) comb block needs to form large microdomains so as to reduce the interfacial curvature for the regular stacking of the smaller-scale lamellae. However, large microdomains could not be formed by the very short P4VP block; therefore, lamellar microdomain becomes the favored structure for enhancing the stacking of the smaller-scale lamellae.

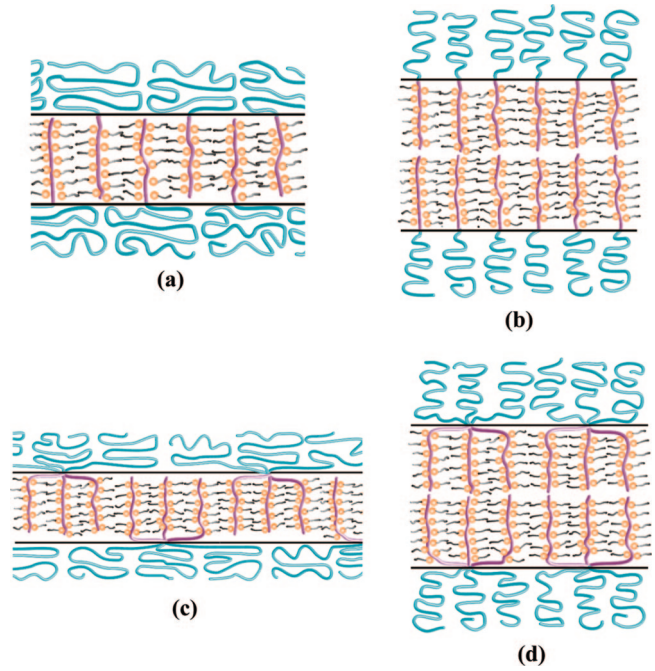

Figure 11. Schematic illustration of the possible arrangements of comb blocks in the comb-coil copolymers: (a) monolayer arrangement in linear architecture; (b) double-layer arrangement in linear architecture; (c) monolayer arrangement in heteroarm star architecture; (d) double-layer arrangement in heteroarm star architecture. The arm number shown in panels c and d is not the real arm number in the heteroarm star copolymers under study.

Additionally, as compared to hydrogen-bonded systems [P4VP(PDP) or P4VP(NDP)] investigated previously with the same composition, DBSA was strongly ionically bound to P4VP in the present systems. In this case, we were dealing with a densely grafted P4VP brush that required a higher interfacial area than the hydrogen-bonded P4VP chains.[44] Thus, a lamellar morphology was more plausible for the present system despite compositional asymmetry.

4. Interdomain Distances of the Larger-Scale Structures. It is clear from Table 2 that the interlamellar distance D of the larger-scale lamellar structure formed by the copolymer domains was larger for the heteroarm star systems than that of their linear counterparts, irrespective of the strength of the surfactant binding. In our previous study of the comb-coil copolymers displaying cylinder-within-lamellae structure, the domain spacing of the larger-scale structure was found to be smaller in heteroarm star copolymers.[15] The smaller D in the star system was attributed to the lower aggregation number of the PS blocks within the cylindrical microdomains due to its peculiar architecture. This finding was different from the previous studies of coil-coil block copolymers[26−30] showing that the star copolymers exhibited a larger domain spacing than the corresponding linear diblock, because the arm crowding near the junction points resulted in strong chain stretching. However, the difference in D found for coil-coil systems was typically less than 15%, while for the present comb-coil systems showing lamellae-within-lamellae morphology the difference was 40−76%. Therefore, the anomalously large D must be caused by other factors.

We propose that the key factor governing the interlamellar distance is the arrangement of the comb blocks forming the smaller-scale lamellar mesophase. Figure 11 shows two possible

types of arrangement, monolayer (ML) and double-layer (DL), of the P4VP(PDP) or P4VP(DBSA) combs in both linear diblock and heteroarm star copolymers. The interlamellar distance associated with the DL arrangement is apparently larger. We propose that the comb blocks in the star copolymer complexes adopted the DL arrangement, whereas those in the linear systems organized as ML. The advantage of adopting a ML arrangement was that the PS blocks could acquire more space to relax because one longer PS block shared the same cross section with two relatively short P4VP(DBSA) combs blocks. The relaxation of PS conformation was entropically favored, but this led to larger interfacial energy due to the larger cross-sectional area. On the contrary, the DL arrangement caused the PS blocks to stretch significantly while it lowered the interfacial energy of the system. In the case of heteroarm star copolymer complex, the effect of entropy may be intrinsically smaller, because the conformational entropy was already lowered by chain crowding as each junction point had to connect several polymer chains together; as a consequence, arranging the comb blocks in ML may not gain much entropic advantage. In this case, the effect of interfacial energy dominated so as to favor DL arrangement. By contrast, the entropic effect became the dominant factor for the linear system, such that the comb blocks adopted the ML arrangement. The calculated cross-sectional area allocated for each PS block (or each comb block), Σ, in both linear and heteroarm star systems, shown in Table 2, indicated that Σ of all star samples was much smaller than that of all linear ones. It should be noted that conclusive evidence of the proposed ML/DL arrangement could be established by investigating the structure as a function of block lengths. Further study along this aspect is underway.

Another interesting observation worth mentioning was that whereas **L1(PDP)** and **L1(DBSA)** displayed about the same interlamellar distance associated with the larger-scale structure, **H1(PDP)** and **H1(DBSA)** showed very different D values (cf. Table 2). This observation could again be explained by considering the architecture effect and also the nature of association of P4VP with PDP and DBSA (hydrogen vs ionic bonding). In the case of H1 copolymer, the crowding at the star junction points significantly affected the chain conformations. In the case of PDP, since the hydrogen bonds were weak and dynamic in nature (continuously broken and formed), it acted more or less like a selective solvent in P4VP domain. However, in the case of DBSA, which was bound to P4VP through a strong ionic bond, the P4VP(DBSA) comb block could be considered as a densely grafted chain. Hence, in H1 copolymer the incorporation of DBSA in P4VP blocks meant significant additional crowding at the junction point because of the DBSA bound to the 4VP unit near the junction point. In this case, the P4VP(DBSA) comb block had to stretch significantly normal to the interface to alleviate this crowding and hence the domain spacing was greater in **H1(DBSA)** than in **H1(PDP)**. This difference was not observed in the case of **L1(PDP)** and **L1(DBSA)** complexes from the obvious fact that the constraint imposed by the junction point effect in heteroarm was absent in the linear copolymer.

Conclusions

The self-assembly behavior of supramolecular comb-coil copolymers has been investigated by use of PS-P4VP copolymers with both linear and heteroarm star architectures complexed with DBSA or PDP. Despite the nonlinear molecular architecture, the heteroarm star comb-coil copolymers exhibited the lamellae-within-lamellae morphology similar to that observed in the linear systems. However, the number of block chains connected to each junction point dominated the balance between conformational entropy and interfacial energy in the copolymer system and resulted in different arrangement of the comb blocks. All heteroarm star copolymers in the present study were proposed to arrange their comb blocks into double layers, while the monolayered arrangement appeared to be more favorable for the comb blocks in their linear counterparts. As a consequence, the interlamellar distances of the copolymer domains in the heteroarm star systems were significantly larger than those associated with the linear diblocks. The junction constraint also influenced both T_{ODT}^{I} and T_{ODT}^{S} of the comb-coil copolymers. Heteroarm star complexes displayed higher T_{ODT}^{I} and T_{ODT}^{S} than linear complexes, irrespective of the binding force of the surfactant to the P4VP block, because of the lower entropy change associated with the ODT values.

Acknowledgment. We gratefully acknowledge financial support from the National Science Council under Contract NSC 96-2221-E-007-023.

Supporting Information Available: Synthetic scheme for heteroarm star PS-P4VP copolymer and GPC characterizations of heteroarm star PS-P4VP copolymer; SAXS heating and cooling profiles of **H1(PDP)**; synchrotron SAXS profiles of **L1(DBSA)**, **L2(DBSA)**, **H1(DBSA)**, and **H2(DBSA)** obtained at room temperature; and SAXS profiles in the high-q region of **L2(DBSA)**. This material is available free of charge via the Internet at http://pubs.acs.org.

References and Notes

(1) Hamley, I. W. *The Physics of Block Copolymers*; Oxford University Press: New York, 1998.
(2) Platé, N. A.; Shibaev, V. P. *Comb-Shaped Polymers and Liquid Crystals*; Plenum Press: New York, 1987.
(3) Antonietti, M.; Conrad, J.; Thünemann, A. *Macromolecules* **1984**, *27*, 6007.
(4) Merta, J.; Torkkeli, M.; Ikonen, T.; Serimaa, R.; Stenius, P. *Macromolecules* **2001**, *34*, 2937.
(5) Ruokolainen, J.; Tanner, J.; Ikkala, O.; ten Brinke, G.; Thomas, E. L. *Macromolecules* **1998**, *31*, 3532.
(6) Chen, H. L.; Ko, C. C.; Lin, T. L. *Langmuir* **2002**, *18*, 5619.
(7) Akiba, I.; Akiyama, S. *Macromolecules* **1999**, *32*, 3741.
(8) Ruokolainen, J.; Tanner, J.; ten Brinke, G.; Ikkala, O.; Torkkeli, M.; Serimaa, R. *Macromolecules* **1995**, *28*, 7779.
(9) Kurth, D. G.; Lehmann, P.; Schütte, M. *Proc. Natl. Acad. Sci. U.S.A.* **2000**, *97*, 5704.
(10) Valkama, S.; Lehtonen, O.; Lappalainen, K.; Kosonen, H.; Castro, P.; Repo, T.; Torkkeli, M.; Serimaa, R.; ten Brinke, G.; Leskelä, M.; Ikkala, O. *Macromol. Rapid Commun.* **2003**, *24*, 556.
(11) Antonietti, M.; Wenzel, A.; Thünemann, A. *Langmuir* **1996**, *12*, 2111.
(12) Hanski, S.; Houbenov, N.; Ruokolainen, J.; Chondronicola, D.; Latrou, H.; Hadjichristidis, N.; Ikkala, O. *Biomacromolecules* **2006**, *7*, 3379.
(13) Ikkala, O.; ten Brinke, G. *Science* **2002**, *295*, 2407.
(14) Nandan, B.; Lee, C. H.; Chen, H. L.; Chen, W. C. *Macromolecules* **2005**, *38*, 10117.
(15) Nandan, B.; Lee, C. H.; Chen, H. L.; Chen, W. C. *Macromolecules* **2006**, *39*, 4460.
(16) Ruokolainen, J.; Mäkinen, R.; Torkkeli, M.; Mäkelä, T.; Serimaa, R.; ten Brinke, G.; Ikkala, O. *Science* **1998**, *280*, 557.
(17) Ruokolainen, J.; ten Brinke, G.; Ikkala, O. *Adv. Mater.* **1999**, *11*, 777.
(18) Valkama, S.; Kosonen, H.; Ruokolainen, J.; Haatainen, T.; Torkkeli, M.; Serimaa, R.; ten Brinke, G.; Ikkala, O. *Nat. Mater.* **2004**, *3*, 872.
(19) Ikkala, O.; ten Brinke, G. *Chem. Commun.* **2004**, *19*, 2131.
(20) Valkama, S.; Ruotsalainen, T.; Nyka1nen, A.; Laiho, A.; Kosonen, H.; ten Brinke, G.; Ikkala, O.; Ruokolainen, J. *Macromolecules* **2006**, *39*, 9327.
(21) Ruotsalainen, T.; Turku, J.; Hiekkataipale, P.; Vainio, U.; Serimaa, R.; ten Brinke, G.; Harlin, A.; Ruokolainen, J.; Ikkala, O. *Soft Matter* **2007**, *3*, 978.
(22) Polushkin, E.; Bondzic, S.; de Wit, J.; Alberda van Ekenstein, G.; Dolbnya, I.; Bras, W.; Ikkala, O.; ten Brinke, G. *Macromolecules* **2005**, *38*, 1804.
(23) Valkama, S.; Ruotsalainen, T.; Nyka1nen, A.; Laiho, A.; Kosonen, H.; ten Brinke, G.; Ikkala, O.; Ruokolainen, J. *Macromolecules* **2006**, *39*, 9327.
(24) Chen, H. L.; Lu, J. S.; Yu, C. H.; Yeh, C. L.; Jeng, U. S.; Chen, W. C. *Macromolecules* **2007**, *40*, 3271.
(25) Voulgaris, D.; Tsitsilianis, C.; Esselink, F. J.; Hadziioannou, G. *Polymer* **1998**, *39*, 6429.

(26) Buzza, D. M. A.; Hamley, I. W.; Fzea, A. H.; Moniruzzaman, M.; Allgaier, J. B.; Young, R. N.; Olmsted, P. D.; McLeish, T. C. B. *Macromolecules* **1999**, *32*, 7483.
(27) Beyer, F. L.; Gido, S. P. *Macromolecules* **1997**, *30*, 2373.
(28) Beyer, F. L.; Gido, S. P.; Uhrig, D.; Mays, J. W.; Tan, N. B.; Trevino, S. F. *J. Polym. Sci., Polym. Phys.* **1999**, *37*, 3392.
(29) Matsen, M. W.; Gardiner, J. M. *J. Chem. Phys.* **2000**, *113*, 1673.
(30) Zhu, Y.; Gido, S. P.; Moshakou, M.; Iatrou, H.; Hadjichristidis, N.; Park, S.; Chang, T. *Macromolecules* **2003**, *36*, 5719.
(31) Hadjichristidis, N.; Iatrou, H.; Tselikas, Y.; Efstratiadis, V. *Chim. Chron.* **1996**, *24*, 189.
(32) Hadjichristidis, N.; Tselikas, Y.; Iatrou, H.; Efstratiadis, V.; Avgeropoulos, A. *J. Macromol. Sci., Pure Appl. Chem.* **1996**, *A33*, 1447.
(33) Tsitsilianis, C.; Voulgaris, D. *Macromol. Chem. Phys.* **1997**, *198*, 997.
(34) Ruokolainen, J.; Torkkeli, M.; Serimaa, R.; Komanschek, B. E.; Ikkala, O.; ten Brinke, G. *Phys. Rev. E* **1996**, *54*, 6646.
(35) Luyten, M. C.; van Ekenstein, G. O. R. A.; ten Brinke, G.; Ruokolainen, J.; Ikkala, O.; Torkkeli, M.; Serimaa, R. *Macromolecules* **1999**, *32*, 4404.
(36) De Wit, J.; van Ekenstein, G. O. R. A.; Polushkin, E.; Kvashnina, K.; Bras, W.; Ikkala, O.; ten Brinke, G. *Macromolecules* **2008**, *41*, 4200.
(37) Vavasour, J. D.; Whitmore, M. D. *Macromolecules* **1992**, *25*, 5477.
(38) Sakurai, S. *Trends in Polymer Science* **1995**, *3*, 90.
(39) Matsen, M. W.; Bates, F. S. *Macromolecules* **1996**, *29*, 1091.
(40) Porod, G. *Kolloid-Z.* **1951**, *124*, 83.
(41) Porod, G. *Kolloid-Z.* **1952**, *125*, 51.
(42) Loo, Y. L.; Register, R. A. *Phys. Rev. Lett.* **2000**, *84*, 4120.
(43) Chen, H. L.; Wu, J. C.; Lin, T. L.; Lin, J. S. *Macromolecules* **2001**, *34*, 6936.
(44) Milner, S. T. *Macromolecules* **1994**, *27*, 2333.

MA801116H